

A description of the vortical skeleton behind an finite-span flapping wing

Parker, K.¹, von Ellenrieder, K. D² and Soria, J¹

¹Laboratory for Turbulence Research in Aerospace & Combustion
Mechanical Engineering, Monash University
Clayton Campus, Victoria, 3800 AUSTRALIA

²Dept. Ocean Engineering
Florida Atlantic University
Dania Beach, FL 33004-3023, USA

Abstract

The structure of the flow behind wings with finite span (3D) is significantly more complex than infinite-span aerofoils due to the presence of wingtip vortices that interact with leading and trailing edge vortices from the 2D case. Besides a qualitative difference in the observed structure, any quantitative topological analysis of the flow structure or of the mechanisms responsible for the interaction of these structures would differ for the two types of bodies. While significant progress has been made in defining the parameter-space of efficient thrust-producing 2D flapping foils, there is still deficiency in understanding the coupled interaction of the phase-specific forced motion with the phase averaged flow structure. Initial qualitative dye flow visualizations have confirmed the difference in the 'wake' structures of a 3D-flapping wing as compared to the general reverse Karman vortex street from 2D aerofoils. (Here 'wake' is used loosely since the reverse Karman vortex street is indicative of velocity addition to the flow, namely thrust production.) These have led to a proposed model representing the 3D vortical skeleton behind a thrust-producing flapping wing. Subsequent 2D PIV analysis provided support for some salient features in the proposed model but is limited in the velocity information it can measure. This paper reports on subsequent stereoscopic PIV measurements at various locations along the span of a symmetrical NACA-profile wing at Strouhal number of 0.35. This paper describes the adopted experimental procedure in order to accurately measure all 3 velocity components, resolve all 3 velocity gradients and calculate the topological information of the flow. Preliminary phase averaged measurements are used investigate the flow topology. Using a stereo- angular displacement configuration, a single phase case is discussed in the context of a proposed model of the three dimensional vortex skeleton of the flow.

Keywords: *Strouhal number, stereoscopic particle image velocimetry, flapping/oscillating airfoil, vortical structures, propulsion, unsteady aerodynamics*

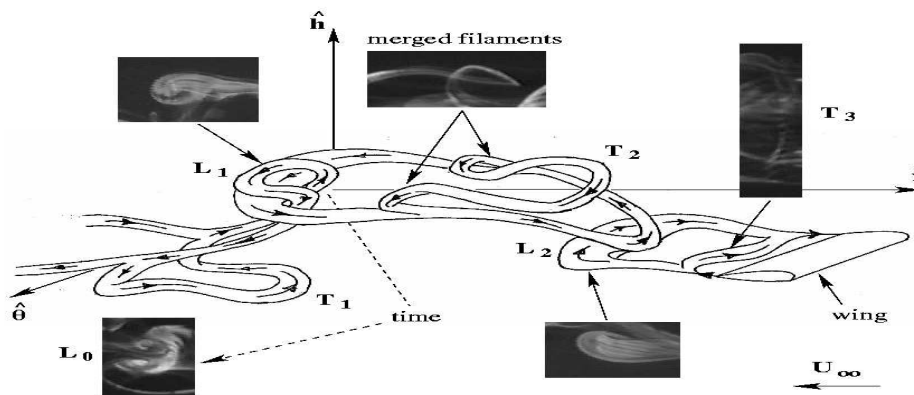


Figure 1: Proposed vortex skeleton behind a 3D flapping airfoil [19].

1 Introduction

The study of oscillating aerofoils has many areas of application. Flapping is described as simultaneous heave and pitch oscillations. Flapping wings or foils are considered as alternate unsteady propulsors to conventional corkscrew-type propellers. Up to 80% thrust efficiency has been recorded for flapping propulsors [1]. The interest in flapping foils emanate from the study of locomotion in certain species of fish, insect and birds. The question is whether any principles from these studies can be applied to engineering applications[5, 18]. The concept of biomimetic engineering does not preclude any complex fluid mechanical refinements which necessitates a greater understanding of the physics responsible, for the assumed optimal efficiency of locomotion in nature.

By understanding the fluid mechanics of flapping wings, we also gain insight into other aero-fluid dynamic problems, specifically in the unsteady flow regime. Aeroelastic flutter is the result of a similar physical dynamic coupled with the elastic nature of the aerostructure [10]. Unsteady loading of turbo-machinery components remains a major problem in the area of power generation. All these areas relate indirectly to vorticity control. In active vorticity control the boundary layer can be manipulated through oscillation of the principal body, or an upstream body or through a tandem arrangement [7, 6]. In these cases the development of the boundary layer and the seperated flow can be modified by regulating the oscillations of the forced body.

Much of our present understanding in this field comes from past experimental [1, 9, 4, 12] and numerical [7, 8, 15]. These studies use aerofoils of infinite-span (2D aerofoils) as the flapping body. While some numerical experiments have studied the effect of wing three dimensionality and flexibility, their focus is primarily on development of an adaptive thin airfoil theory for prediction of thrust on flapping wings [8]. The dimensionless Strouhal number has been identified as a suitable parameter to describe the thrust producing ability of a flapping foil. In a Strouhal regime of $0.25 \leq St \leq 0.35$ 2D aerofoils produce thrust with maximum efficiency. Strouhal number, St is defined as,

$$St = \frac{fA}{U_\infty}, \quad (1)$$

where f equals the frequency of oscillation (heave frequency equals pitch frequency), A represents the maximum excursion of the airfoil trailing-edge (= double-amplitude of oscillation, = c) and U_∞ represents the free-stream velocity. The flow behind a thrust producing foil is described by a 'reverse' Karman vortex street in which the mean velocity profile resembles a jet and momentum is added to the flow. In reality, wings are three dimensional and have finite spans. In this case the wingtip vortices add another dimension of complication to the vortical interactions and structure of the flow. Cheng and Murillo [2] first raised concerns that results from studies on 2D aerofoils were over-estimated. Figure 2a shows a typical qualitative flow visualizations as observed from the wingtip of the aerofoil. In contrast, the presence of wingtip vortices significantly alter the typical 2D vortex sheet shown as shown in figure 5a. Here the structure of the flow, at the same operating conditions is significantly more three dimensional and complex than the 2D case. In both cases the $St = 0.35$ and the images were taken at the same heave and pitch locations of a NACA0030 aerofoil. A parametric dye-flow visualization study by the present authors have resulted in a model of the vortical skeleton for the thrust producing case [19]. A sketch of the proposed vortex skeleton is shown in figure 1. The L and T labels in the figure represents a vortical structure seperating of the airfoil from the leading or trailing edge respectively. The subscripts 1,2 and 3 represent the respective pair of vortical structures to which L or T belong. Since dye is a passive scalar and flow visualizations in an unsteady flow are ambiguous in the information that they provide, more quantitative experiments are necessary.

The results presented in this paper are part of a larger study to identify the structures in a complex 3D 'jet' of a thrust producing wing. The interaction of these structures is described in the context of the proposed generic skeleton in figure 1. Of interest is the relationship between the phase-locked structure and the forced oscillation. The study focusses on two aspects; 1) The effect on vorticity control, and 2) the effect on the ability to produce thrust. To carry out a topological reconstruction, accurate and complete information about the velocity gradient tensor is required [3]. To understand the dynamics of this unsteady flow caused by relatively large external periodic forcing, a phase-averaged approach is used. To this end this paper reports on phase averaged stereoscopic PIV measurements. The stereo-measurements provide quantitative three-component data of the trailing edge flow. One phase condition in the oscillating trajectory of the wing is presented here as part of the refinement process of acquiring

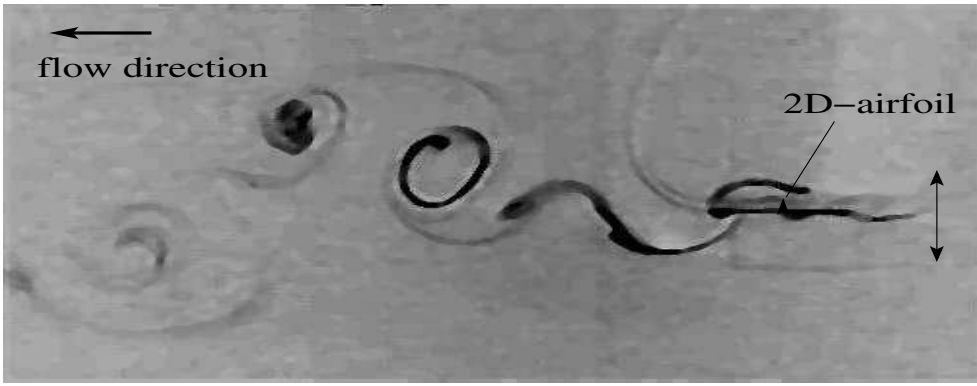


Figure 2: Dye flow visualization of the flow behind a 2D flapping aerofoil.

accurate stereo velocity measurements of this flow. The inherent radial-distortion difficulties associated with stereoscopic registration through liquid-air interface is considered.

2 Experimental Technique

2.1 Apparatus & method

The experiments are conducted in a water tunnel at the Laboratory for Turbulence Research for Aerospace & Combustion. The tunnel has 5 working sections measuring $500\text{mm} \times 500\text{mm} \times 1000\text{mm}$ each. The turbulence intensity levels in the operated test section is less than 0.35% at the freestream velocity of 92mm/s . Figure 3 illustrates the experimental layout.

In order to compare the results to the model proposed by von Ellenrieder *et al* [19], a similar NACA0030-type aerofoil with chord, $c = 20\text{mm}$ and $AR = 3$ is suspended vertically above the test section as shown in figure 3. The aerofoil performs angular (pitch) and lateral (heave) oscillations using stepper motors. The aerofoil heaves in the y direction and simultaneously pitches about the quarter-chord position. The heave-stepper motor performs the oscillations by virtue of a scotch yoke mechanism. The scotch yoke wheel can be adjusted to accommodate different heave oscillation amplitudes. The scotch yoke arm reciprocates a platform which is mounted on bearings. The motor responsible for aerofoil pitch oscillations is mounted on this platform. The pitch motor drives the aerofoil directly. A motion control program was developed in-house in such a manner to allow different motion parameters (such as frequency, f , maximum pitch oscillation amplitude, θ_0 and phase angle between heaving and pitching oscillations, ψ) to be independently varied. Thereby allowing for various motion profiles.

The entire oscillating mechanism is mounted on a railing system above the water tunnel, allowing the aerofoil setup to be moved to different streamwise locations, while the cameras and laser arrangement is kept fixed. For this study, the trajectory of the foil study resembles a cosine curve in which,

$$h(t) = h_0 \cos(\omega t), \quad (2)$$

$$\theta(t) = \theta_0 \cos(\omega t + \psi), \quad (3)$$

where, $h_0 = c/2$ and $\omega = 2\pi f$ (equal for heave and pitch oscillations). These parameters are chosen since they produce thrust optimally in 2D aerofoils [1] and at these operating conditions, the 'jet' structure is significantly altered for a 3D foil [19].

Potentiometers are mounted along the heave and pitch axes. These provide accurate feedback of the output motion trajectory of the foils. Optical triggers have been placed at the $h = 0$, $h = h_0$ and $\theta = \theta_0$ locations to provide the trigger signals to the laser and cameras. For any experiment the image acquisition system remains fixed on an optical table, while the airfoil is able to move up or down a translation stage to allow for different spanwise measurements. The airfoil can be accurately translated up to 0.025mm .

2.2 Data Acquisition

In order to quantitatively analyze the flow, digital particle image velocimetry is utilized. PIV measurements are conducted in the near wake region of the foil. A region $4c$ (y-direction) by $3c$ (x-direction) is captured at a magnification of 0.1. Previous flow visualizations by Parker *et al* [14] suggest that this measurement area is adequate to capture the large scale structures in the flow over 1 complete forced oscillation cycle of the foil.

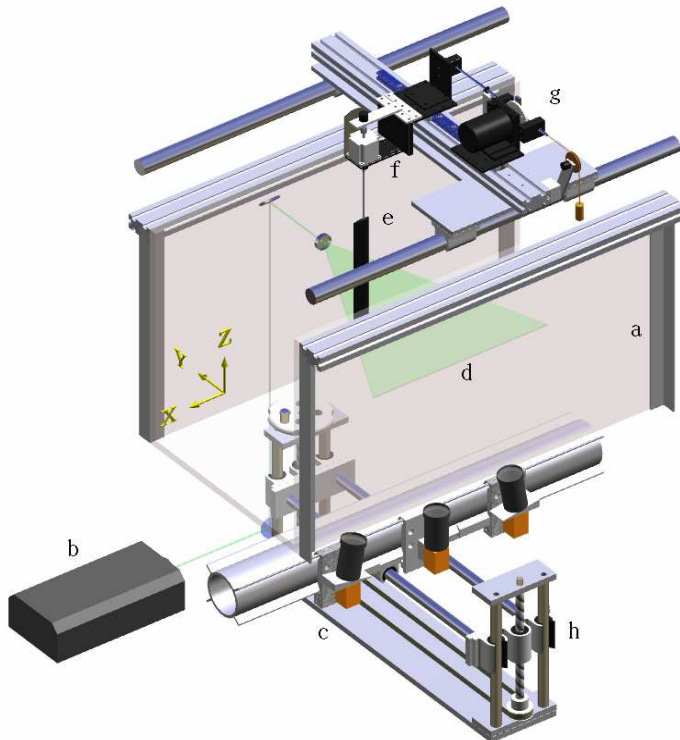


Figure 3: Schematic of the experimental apparatus: a) test section, b) laser, c) stereo-CCD camera arrangement on 3-axis translation stage, d) vertical light sheet, e) wing f) pitch stepper motor, g) heave stepper motor with scotch-yoke.

As shown in figure 3, three Pixelfly CCD cameras, with array sizes of $1280px \times 1024px$ each, are mounted vertically onto a 3-axis translation stage, below the test section. An angular-displacement stereo-configuration is utilized with the stereo-cameras at 68° to each other. This angle is within an acceptable range for minimising the total error in the stereo-measurement [11]. The centre camera is used for standard 2D PIV and is used as a 'check' of the quality of the freestream flow as well as fine tuning all the PIV setup parameters. It also provides a useful and simple check for the individual stereo-PIV data. The three cameras are setup in such a manner that the only difference is the added distortion in the stereo cameras. The cameras are fitted with $55mm$ Micro Nikkor Nikon lenses. During the stereo acquisition the aperture is operated at $f\#11$ to increase the ability to focus on the particles. For 2D-PIV $f\#2.8$ is used for maximum light intensity. To satisfy the Schiempflug condition and get uniform focus in the distorted stereo images, each camera axis is tilted by 3° . $11\mu m$ hollow glass fibre beads are used to seed the water tunnel. The particles are illuminate by a laser light from a dual-cavity New Wave Nd:Yag laser, pulsing $532nm$ light at $32mJ$. With the necessary optics, a $3mm$ thick horizontal light sheet is created in the midspan region of the aerofoil (see figure 3). A beam collector is placed on the far side wall of the test section to collect light from the laser.

2.3 Stereo Acquisition

An in-situ calibration technique is utilized [16], using a $250mm$ -square plate with an array of $0.5mm$ through-holes (calibration markers) drilled at $5mm$ spacings. Calibration images are acquired for each camera at five equally-spaced planes across the thickness of the laser sheet from $-1.5mm \leq z \leq +1.5mm$.

During acquisition of the calibration images the calibration plate is illuminated from the back with a light box providing a black calibration image with white dots. Using a template-matching digital image correlation scheme, the exact locations of calibration markers in distorted image space are found. This arrangement was found to give a good Gaussian dbn of light intensity and provide high correlation for locating the centre of the calibration markers with a rms mapping error less than 0.3px for x co-ordinate 0.2px for y co-ordinate . A polynomial with cubic dependence on the in-plane components, x and y and quadratic dependence on the out-of plane component, z is used to map the displacement in the undistorted object plane to an image plane displacement. This is found to be adequate to remove any higher order distortions one expects to encounter [16]. A least squares approach is used to determine the mapping function for the cameras and also to calculate the final displacements of the flow field.

The residual error is an indicator of the ability of the stereo-reconstruction algorithms to accurately determine the displacements from [19] the two cameras by passing the derived measurement back through the system and re-calculating the initial input from each camera. This provides a measure of the residual noise contributed by the mathematical system. For these experiments the residual error was 0.006px, 0.02px for camera1, component x and y. For camera 2, the residual error for x was 0.005px and y, 0.03px. The stereo reconstruction algorithm, StereoMagik[©], is able to resolve 10px displacement with an rms error of 0.06px for the in-plane components and 0.09px for the out of plane component.

In order to provide a volumetric measure of the velocity data, double exposed images are acquired in several planes along the span of the wing (z -direction). The laser firing is synchronized with the motion of the wing. A trigger signal from a stepper motor is sent via a breakout box, to a RT Linux control computer that regulates a return signal to activate the laser firing and the camera acquisitions. Figure 4 shows the basic acquisition sequence.

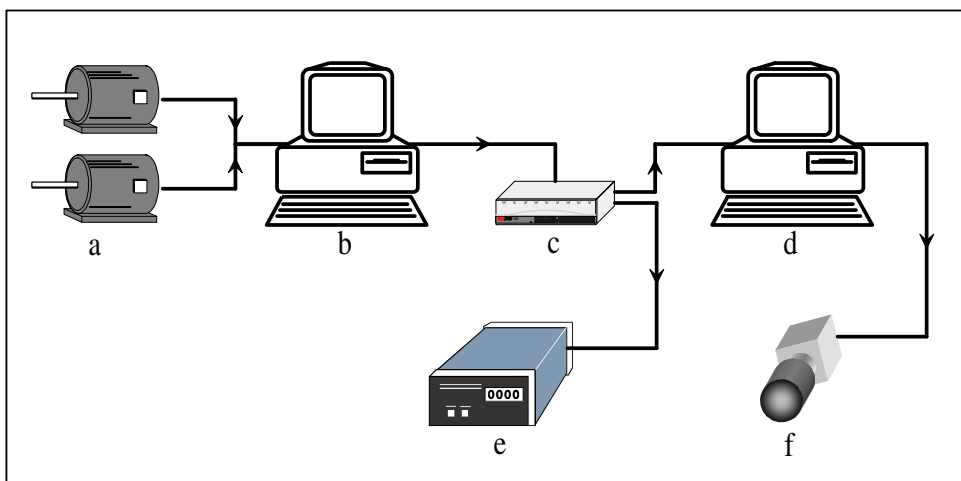


Figure 4: Schematic of the image acquisition system for the stereo experiments

Phase-averaged measurements are made at 8 locations within 1 heave cycle. The period of 1 heave cycle is $620ms$. Based on the variance in the measured velocity 1000 instantaneous images are taken to achieve velocities with 1% error based on a statistical confidence of 99%. The acquired image pairs are analyzed using an adaptive multigrid cross-correlation algorithm from Soria [17]. From the stereo images, the three components of velocity u, v and w and the out of plane vorticity, (ω_z) is derived from the velocity gradients. From the instantaneous velocity fields, the mean velocity field are calculated at specific phases in the heave cycle of the wing.

3 Discussion of Results

Preliminary 2D PIV measurement at the plane of symmetry of the aerofoil reveal information about the vortical shedding pattern and relative strength of vorticity in the imaged plane [13]. As figure 5b shows, pairs of vortices are shed from the aerofoil surface in an arrangement not unlike the Karman vortex street. This measurement is taken at the midspan of the airfoil. There are several structures in the flow. Here the velocity vector field has been shaded by the out-of-plane vorticity non-dimensionalised by the

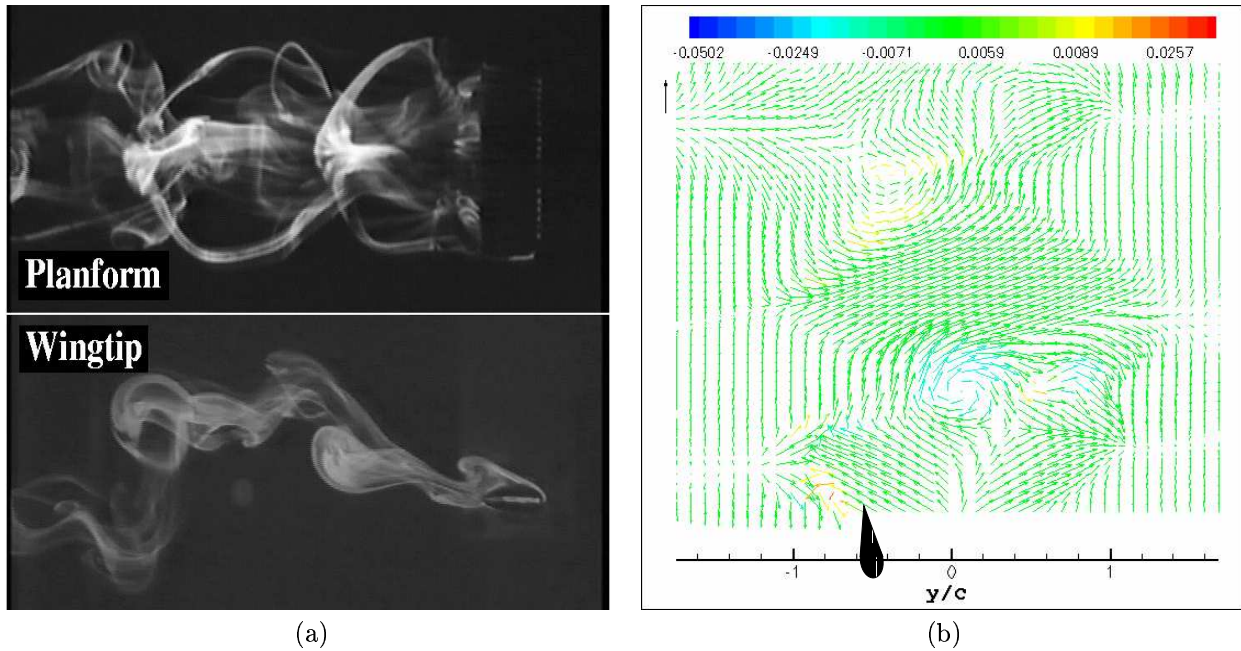


Figure 5: a) Dye flow visualisation of the flow behind a 3D flapping foil. b) 2D PIV measurements of the flow behind a 3D flapping foil. Flow is from top to bottom. x-axis is non-dimensionalised by the aerofoil chord length c ($= 2h_0$), double the heave oscillation amplitude.

maximum angular velocity of the flapping foil, (ω_z/ω_θ) . The convection velocity has been subtracted from the phase-averaged field to give a frame of reference moving with the flow. The orientation of the aerofoil relative to the flow is highlighted by the aerofoil sketch at the bottom of the image. For the phase shown, (phase 0) the airfoil has reached the maximum heave amplitude location with a pitch angle of 0° . The flow is complex and the information that can be gathered from a single 2D-2C measurement of a three dimensional flow, is limited and ambiguous. The flow visualizations in figure 5a suggest that the vorticity shed from the leading edge, trailing edge and wingtips are connected. There is considerable span-wise movement. Thus, any planar measurement will experience ambiguity due to strong out-of-plane motion. Consequently, three component, three dimensional measurements are necessary to describe the flow structure and check the proposed vortex skeleton model [19].

The results for the case of $Re = 3000$, $\psi = 90^\circ$, $\theta_0 = 5^\circ$ and $St = 0.35$ is presented. From figure 5a it is possible to get an idea of the extent of the measurement area required in the PIV experiments in order to capture the large scale structure of the flow. For all the images that follow the axes have been non-dimensionalised by the aerofoil chord length c ($= 2h_0$), double the heave oscillation amplitude. As a result of oblique visualisation of the flow by the CCD cameras, through 25mm perspex, 300mm fluid and air, the radial distortion created asymmetrical focus and distortion across the object plane, even with the Schiemiug condition established. By repeating the calibration and acquisition process several times for a single experiment it was possible to acquire acceptable data. An increase in the lense $f\#$ improved the ability to focus particles at the expense of increased laser intensity.

Figure 3a shows the distribution of the resolved out-of-plane velocity component, w in the measured plane. The magnitude of the velocity shows regions where the flow is in and out of the plane. The measured plane is the plane of symmetry which in figure 5a is the centre of the airfoil span. For the phase case shown, the wing has reached $-h_0$ and is changing direction to move upwards in the image. In the region close to the trailing edge of the wing, figure 3b shows a structure of relatively strong positive vorticity. There is a co-rotating pair following the trailing edge vortex.

More planes of measurement are required to interpret these regions in the flow to the topology observed in figure 5a. Figure 7a shows the topology through an integrated streamline pattern of the in-plane velocity components, u, v . The convection velocity, u_∞ has been removed to obtain a frame of reference moving with the flow. Immediately observable are two critical points. these foci bear 'some' resemblance to the trailing edge structures described in the model of von Ellenrieder *et al*[19] but this claim necessitates further topological analysis across more planes of the wing span. The 3 components of velocity have been

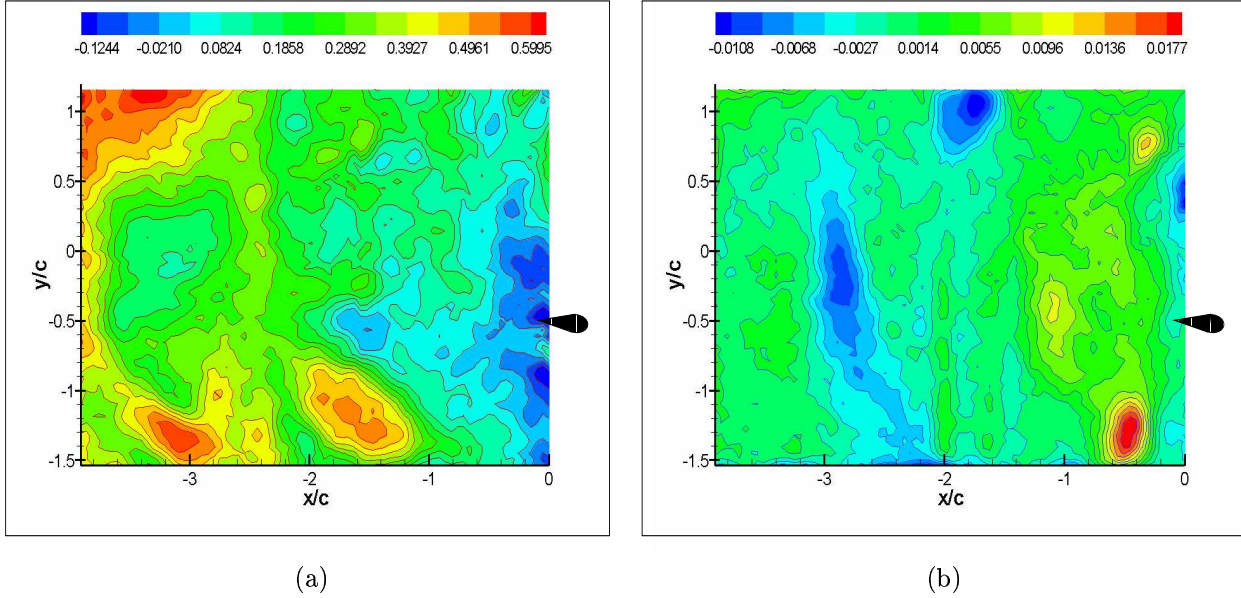


Figure 6: a) Out-of-plane, w velocity component contour of the flow behind a 3D flapping foil. Velocity magnitude is non-dimensionalised by the freestream velocity, u_∞ . b) Contour plot of the out of plane vorticity ω_z/ω_θ , where vorticity is non-dimensionalised by the angular velocity of the pitching oscillation of the flapping foil.

represented on a single plot in figure 7b, to give a sense of the variation in the flow topology due to the z -component of velocity. Evidently, the w -velocity becomes larger as the flow convects further downstream of the wing.

Figure 8 and figure 9 represent the non-dimensional variances of the 3 measured velocities from the mean. The variance in the in-plane components is relatively minor compared to the out-of-plane component. In regions with higher velocity gradients the variances differ by a factor of 4.

4 Summary

Qualitative flow visualisations have resulted in the formulation of a model for the vortical skeleton behind a three-dimensional thrust-producing flapping foil. To test the model sufficient quantitative information is required of all the velocity components. It is proposed to use a method of invariants of the velocity gradient tensor [3] to resolve the vortical structures that constitute the topology. Stereoscopic PIV measurements are able to give 3 components of velocity in a single plane. It is proposed to use multiple planes to calculate the velocity gradients. Preliminary stereo-measurements have been used to refine the experimental technique. These results have been presented for a single phase and experiments are planned for other phases. This will be used to create a phase related picture of the flow evolution. To correct for the huge radial distortions and provide more uniform focussing in the object plane, it is proposed to use a liquid filled prism.

5 Acknowledgement

The authors would like to acknowledge the support of Dr. Phillipa O'Neil and Dr. Simon Clarke in the formulation of the stereo reconstruction algorithm. Also Mr. Ivor Mackay, Mr. Eric Wirth and Mr. Adam Castle for the fabrication of the experimental rig.

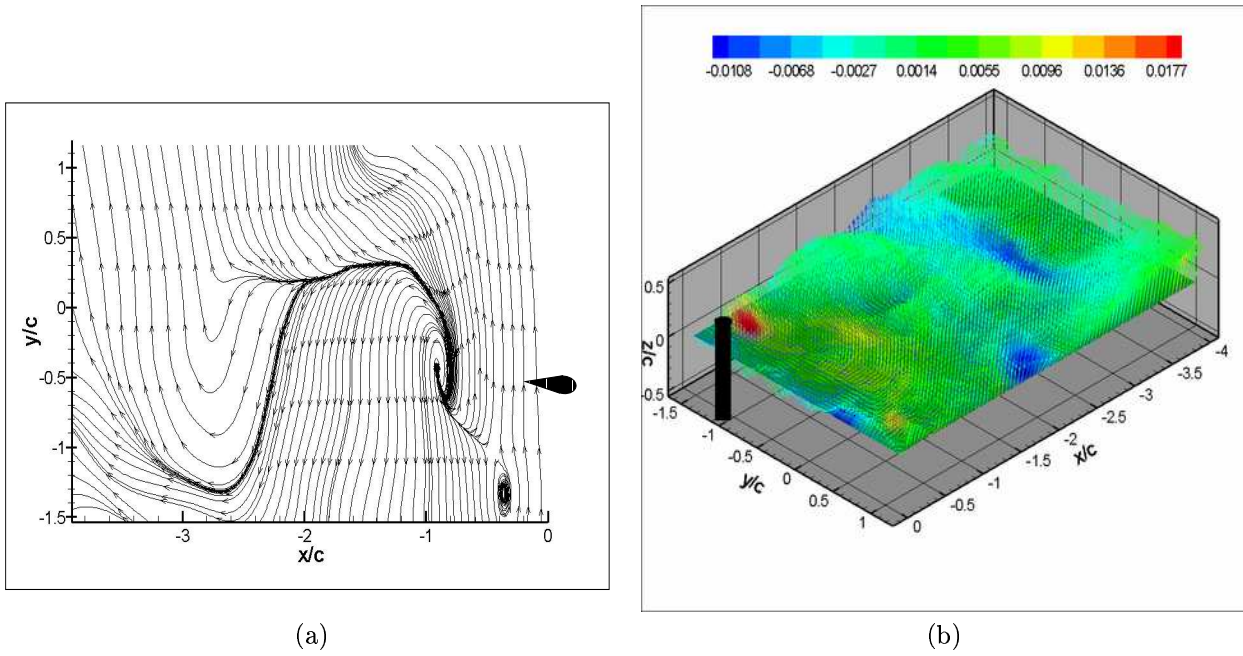


Figure 7: a) Streamline pattern of the u and v velocity components of the flow behind a 3D flapping foil. Velocity magnitude is non-dimensionalised by the freestream velocity, u_∞ . b) Three-component velocity vector field. u -velocity in x axis, v -velocity in y axis and w -velocity in z axis.

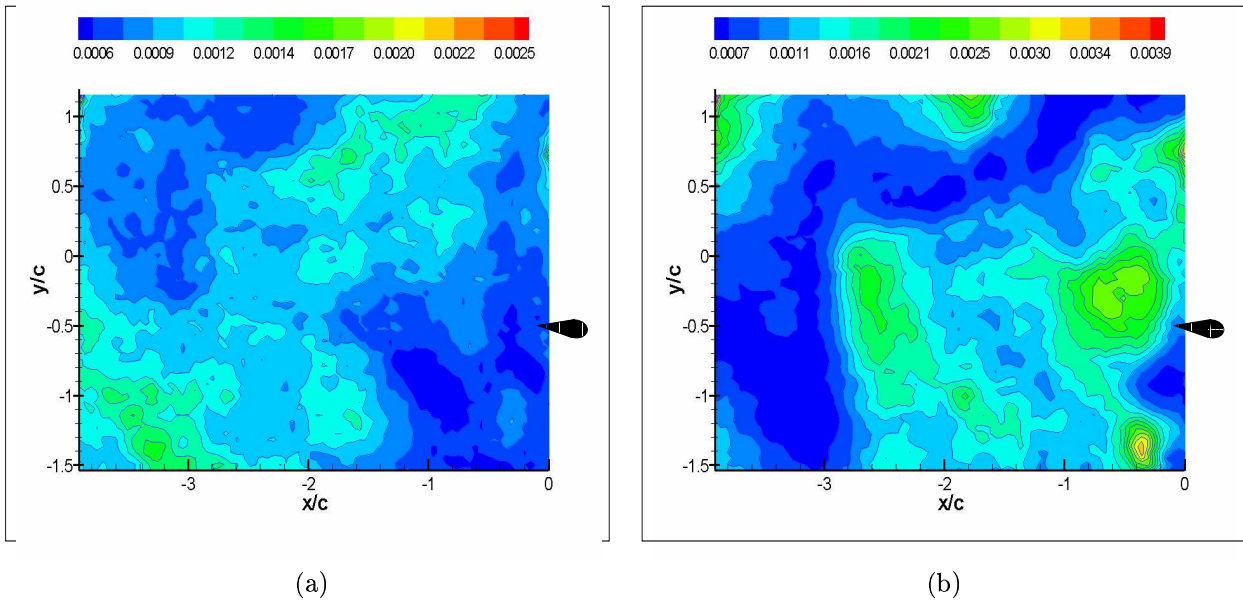


Figure 8: a) Mean square error in the u -velocity component. b) Mean square error in the v -velocity component. In a) and b) velocity magnitude is non-dimensionalised by the square of the freestream velocity, u_∞^2 .

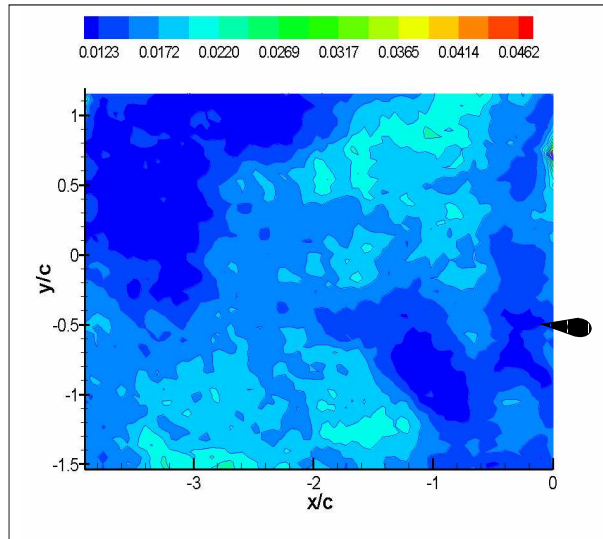


Figure 9: Mean square error in the w-velocity component. Velocity magnitude is non-dimensionalised by the square of the freestream velocity, u_∞^2 .

References

- [1] J. M. Anderson, K. Streitlien, D. S. Barrett, and M. S. Triantafyllou. Oscillating foils of high propulsive efficiency. *J. Fluid Mech.*, 360:41–72, 1998.
- [2] H. K. Cheng and L. E. Murillo. Lunate-tail swimming propulsion of curved lifting line in unsteady flow. part 1. asymptotic theory. *J. Fluid Mech.*, 143:327–350, 1984.
- [3] M.S. Chong, A.E. Perry, and B.J. Cantwell. A general classification of three-dimensional flow fields. *Phys. Fluids*, 2(5):765–777, May 1990.
- [4] J. D. DeLaurier and J. M. Harris. Experimental study of oscillating-wing propulsion. *J. Aircraft*, 19(5):368–373, May 1982.
- [5] Lauder G. V. Drucker E. G. Locomotor forces on a swimming fish: three-dimensional vortex wake dynamics quantified using digital particle image velocimetry. *J. Exp. Biology*, 202:2393–2412, 1999.
- [6] R. Gopalkrishnan, M. S. Triantafyllou, G. S. Triantafyllou, and D. Barrett. Active vorticity control in a shear layer using a flapping foil. *J. Fluid Mech.*, 274:1–21, 1994.
- [7] K. D. Jones, C. M. Dohring, and M. F. Platzer. Experimental and computational investigation of the Knoller-Betz Effect. *AIAA J.*, 36(7):1240–1246, July 1998.
- [8] K. D. Jones and M. F. Platzer. Numerical computation of flapping wing propulsion and power extraction. *AIAA Paper No. 97-0826*, 1997.
- [9] Chen H. K. Karpouzian G., Spedding G. Lunate-tail swimming propulsion. *J. Fluid Mech.*, 210:329–351, 1990.
- [10] J. Katz and D. Weihz. Behaviour of vortex wakes from oscillating airfoils. *J. of Aircraft*, 50(12):861–863, 1978.
- [11] N. J. Lawson and J. Wu. Three-dimensional particle image velocimetry: error analysis of stereoscopic techniques. *Meas. Sci. Technol.*, 8:1455–1464, 1997.
- [12] K. Ohmi, M. Coutanceau, T. P. Loc, and A. Dulieu. Further experiments on vortex formation around an oscillating and translating foil at large incidences. *J. Fluid Mech.*, 225:607–630, 1991.

- [13] Soria J. Parker K., von Ellenrieder K. D. A quantitative analysis of the structure of the flow behind a thrust producing three-dimensional heaving and pitching foil. In *Proc. 3rd International Conference Heat Transfer, Fluid Mechanics and Thermodynamics, South Africa*, HEFAT, June 21-24 2004.
- [14] Soria J. Parker K., von Ellenrieder K.D. The effects of phase angle on the vortical signatures behind a flapping airfoil of finite aspect ratio. In *Proc. 10th Intl. Symp. Flow Visualization*, August 2002.
- [15] R. Ramamurti and W. C. Sandberg. Computational study of 3-d flapping flows. *AIAA Paper No. 2001-0605*, 2001.
- [16] Liu Z. C. Soloff S. M., Adrian R. J. Distortion compensation for generalized stereoscopic particle image velocimetry. *Meas. Sci. Technol.*, 8:1441–1454, 1997.
- [17] J. Soria. Multigrid approach to cross-correlation digital PIV and HPIV analysis. In *Proceedings of 13th Australasian Fluid Mechanics Conference*. Monash University, 1998.
- [18] G. S. Triantafyllou, M. S. Triantafyllou, and M. A. Grosenbaugh. Optimal thrust development in oscillating foils with application to fish propulsion. *J. Fluid Struct.*, 7:205–224, 1993.
- [19] Soria J. von Ellenrieder K. D., Parker K. Flow structures behind a heaving and pitching finite-span wing. *J. Fluid Mech.*, 490:129–138, 2003.